International Journal of Concrete Structures and Materials

RESEARCH

Study on Deterioration Characteristics and Fracturing Mechanism of Concrete Under Liquid Nitrogen Cold Shock

Jialiang Liu[1,2,3*], Yu Jin[1,2], Yujie Zhu[1,2], Jinyang Li[1,2], Xuguang Zhang[4] and Chao Tao[5]

Abstract

High-pressure water jet crushing concrete has significant advantages in safety, quality and environmental protection, which has a broad application prospect in the maintenance and reconstruction of concrete building. Nevertheless, it still has some problems such as high threshold pump pressure and large specific energy consumption. Water jet breaking concrete with liquid nitrogen (LN_2) cold shock assistance combined with the low-temperature-induced fracturing and hydraulic impact can effectively reduce the working pressure of water jet and improve the energy utilization rate. On account of the unclear cracking characteristics and mechanism of concrete under the LN_2 cold shock, this research carried out the following systematic research focusing on the key scientific issues above based on mechanical tests, scanning electron microscopy (SEM), and nuclear magnetic resonance (NMR). Results indicate that the total mass of concrete exfoliated blocks after compression failure increases as the LN_2 cold shock time and the number of shock cycles goes up, and the uniaxial compressive strength decreases from 8.27 to 21.96%. Through SEM and NMR analysis, it is found that LN_2 cold shock can cause more micro-cracks to develop inside the concrete, and the pore development increases as the cold shock time and the cycle number increase. Additionally, under the condition of water jet pump pressure of 150 MPa, the maximum width and depth of crater for cold shock of 5 min increase by 41.79% and 20.48%, respectively, and those for cold shock of 10 min increase by 76.72% and 40.43%, respectively, compared with the original sample.

Keywords: liquid nitrogen cold shock, scanning electron microscopy, nuclear magnetic resonance, fracturing mechanism

1 Introduction

Concrete structure is the main component of buildings. Due to design defects, long-term high load carrying, poor geological environment or natural disasters, it is necessary to maintain and reform the structures that may have damage or disease in concrete facilities. Traditional mechanical crushing methods have many defects in crushing quality, safety and environmental protection.

The high-pressure water jet crushing technology breaks through the traditional mechanical methods, which have the advantages of high efficiency, no pollution, and selective destruction. Nevertheless, there are problems in the application process of the high-pressure water jet technology such as high threshold pump pressure, high specific energy consumption of crushed materials, and uncontrollable fracturing, which restricts the further development of this technology.

Water jet breaking concrete with liquid nitrogen (LN_2) cold shock assistance is that ultra-low temperature LN_2 acts on concrete to make it cool rapidly and form large thermal stress inside, which induces cracks in the structure with higher integrity. For the high-pressure water

*Correspondence: liujialiang@cqjtu.edu.cn
[1] State Key Laboratory of Mountain Bridge and Tunnel Engineering, Chongqing Jiaotong University, Chongqing 400074, People's Republic of China
Full list of author information is available at the end of the article

Liu *et al. Int J Concr Struct Mater*   (2021) 15:49

Page 2 of 12

jet impacting concrete, the impact, erosion, and wedge effect of the high-pressure water can drive the cracks to expand, finally forming a large and perforated crack network, thereby effectively breaking and dismantling concrete structures. The coupling method of LN_2 cold shock and water jet impact combines significant technical advantages each other, which can shift the cracking effect, effectively reduce the integrity of concrete, and greatly improve the crushing efficiency. But the coupling method involves the problems of fluid–solid coupling, nonlinear dynamic collision and thermal conduction, and complicated failure mechanism of concrete. For example, the failure law of concrete under the coupling action and the matching and optimization of parameters are still unclear. The solution to the above problems is based on the in-depth study of concrete deterioration characteristics and cracking mechanism under LN_2 cold shock.

In recent years, many scholars have carried out a lot of researches on the macro- and micro-properties of materials such as concrete, rock and coal at different temperatures.

Research on ultra-low temperature cold shock concrete, Marshall, (1982) reviewed the low-temperature behavior of concrete and demonstrated possible relationships between compressive strength, tensile strength and elasticity. Cha et al., (2014) compared the cryogenic fracturing results from unstressed weak concrete and sandstone, the characteristics of crack generation are obtained. Jiang et al., (2020) based on the phase transformation process and structural characteristics of pore water in concrete at cryogenic temperature, the mechanical properties at cryogenic temperature are analyzed and summarized. Zhu et al., (Zhu, Jiang, et al., 2020; Zhu, et al., 2020) used atomic force microscope (AFM), XRD and other equipment to study the morphological characteristics, nanomechanical properties, and volume stability of C–S–H grains and the basic building blocks under cryogenic attack.

Research on other temperature of concrete, Penttala et al., (2002) conducted the freezing and thawing experiments of two types of concrete cured under water and at 96% relative humidity and studied the mechanical properties of them based on thermodynamics and the linear theory of elasticity. Thomas et al., (2019) used the three-dimensional digital image method to explore the mechanical properties of concrete at low temperatures. Hartell et al., (2020) comparatively analyzed the degradation mechanism of concrete at four different temperatures and detected the damage process during loading using acoustic emission technology. Hou et al., (2020) used Weibull-lognormal theory to fit the stress–strain curve of low-temperature concrete under multiple conditions and established a dynamic axial compression

constitutive model of concrete under freezing conditions. Pu et al., (2020) comparatively tested the fracture energy of concrete under the three factors of different water–binder ratio, air content and fly ash content.

Research on ultra-low temperature cold shock rock or coal, Cai et al., (2014) inspected the pore structure of rock before and after LN_2 cooling, and analyzed the influence of rock type and water content on the change of pore structure. Huang et al., (2016) used LN_2 to freeze rocks in different water-bearing states and analyzed the influences of low temperature on the mechanical properties of rocks. Zhai et al., (2016, 2020) used nuclear magnetic resonance (NMR) and strain monitoring technologies to study the structural changes of coal when the coal samples were treated with LN_2 at low temperature and analyzed the pore evolution characteristics of coal under low temperature. Cheng et al., (2017) studied the effect of LN_2 on the pore structure and mechanical properties of stratified coal through permeability tests, ultrasonic tests and triaxial compression tests. Qin et al., (2017) explored the petrophysical properties of coal with different LN_2 freezing time and freeze–thaw cycles based on the NMR technology. Yuan et al., (2020) used NMR equipment to test the T_2 atlas of saturated coal samples after LN_2 freeze–thaw cycles and analyzed the influence of coal rank and freeze–thaw cycles on the cracking effect of LN_2 freeze–thaw cycles. Zhang et al., (2021) performed LN_2 cycle freeze–thaw treatments on coal samples with different water contents, and used a camera to observe the evolution of macroscopic cracks on the surface of the coal samples in each cycle.

Research on rock or coal under other temperature condition, Abdulagatova et al., (2019) used laser flash method and differential scanning calorimeter to study the influence of temperature on the thermophysical properties of natural reservoir rocks. Yang et al., (2020) analyzed the influence of negative temperature on rock strength, fractal dimension and dissipation energy through the dynamic mechanical properties of red sandstone under negative temperature, and revealed the deterioration mechanism of dynamic mechanical properties of rock at lower negative temperature by exploring the microscopic fracture morphology. Justo et al., (2020) tested the mechanical properties of rocks at different temperatures and studied the evolution characteristics of the tensile strength and fracture toughness of four different types of rocks with different temperatures.

The above scholars provide a necessary research basis for this study in the aspects of physical property changes and micromorphology of concrete under low-temperature cold shock, but the research involving the mechanical failure characteristics of concrete before and after the cold shock of LN_2 and the internal microscopic

Liu *et al. Int J Concr Struct Mater*   (2021) 15:49

Page 3 of 12

failure characteristics are not comprehensive and specific enough. Although the mechanical properties and internal pore changes are involved in the cold shock of rock and coal by LN_2, concrete is a multi-component, multi-scale and multiphase composite material. Compared with rock and coal, its components are more complex, and the failure characteristics and failure mechanism after LN_2 cold shock are different. Therefore, combined with mechanical test, scanning electron microscope (SEM) and nuclear magnetic resonance (NMR) technology, this paper reveals the changes of mechanical properties, internal micro-failure characteristics and internal pores of concrete before and after LN_2 cold shock. At the same time, the failure mechanism under the combined action of temperature stress and freeze–thaw force is studied. Combined with the test, failure characteristics of water jet before and after LN_2 cold shock are analyzed from the macro-point of view. The research results can provide an important theoretical basis for LN_2 cold shock concrete technology, and have important theoretical significance and engineering value for promoting the application of this technology in the field of concrete crushing.

2 Macro–Micro Failure Characteristics of Concrete Before and After LN_2 Cold Shock

2.1 Experimental Equipment
This paper mainly compared and analyzed the concrete strength, internal micro-failure characteristics, and pore characteristics before and after LN_2 cold shock. The primary devices used in the experiment include LN_2 tank, pressure testing machine, SEM device and NMR test system. To study the influence of LN_2 on the compressive strength of concrete, a WHY-3000 microcomputer-controlled pressure testing machine produced by Shanghai Hualong Test Instruments Corporation, China, was used to carry out a uniaxial compressive test of concrete. The German Zeiss ZEISS field emission SEM SIGMA 300 was utilized for SEM experiments to explore the microscopic morphology of the concrete surface before and after LN_2 cold shock. The NM120-025 V-1 NMR test system of Suzhou Niumag Analytical Instrument Corporation, China was utilized for NMR test to study the expansion of micro-cracks in the concrete before and after LN_2 cold shock. The specific experimental procedure is shown in Fig. 1.

2.2 Uniaxial Compression Experiment
2.2.1 Sample Preparation
Research objects are the same batch of C30 concrete samples, prepared according to the P.R.C Standards "GB/T50081-2019", the mixture proportion is water:cement (ordinary Portland cement 32.5 R):sand:stones (5–20 mm)＝0.38:1:1.11:2.72. After the specimen was casted, they were cured in a standard curing room (20±2 ℃, 95% relative humidity) for 28 days, and then the specimens were taken out for LN_2 cold shock test. After the sample was returned to environmental temperature, the mechanical experiment was carried out. For the convenience of concrete sample numbering, the original sample number is S_0, the concrete sample number of LN_2 cold shock for 5 min is S_{5min}, and the concrete sample number of LN_2 cold shock for 10 min is S_{10min}. LN_2
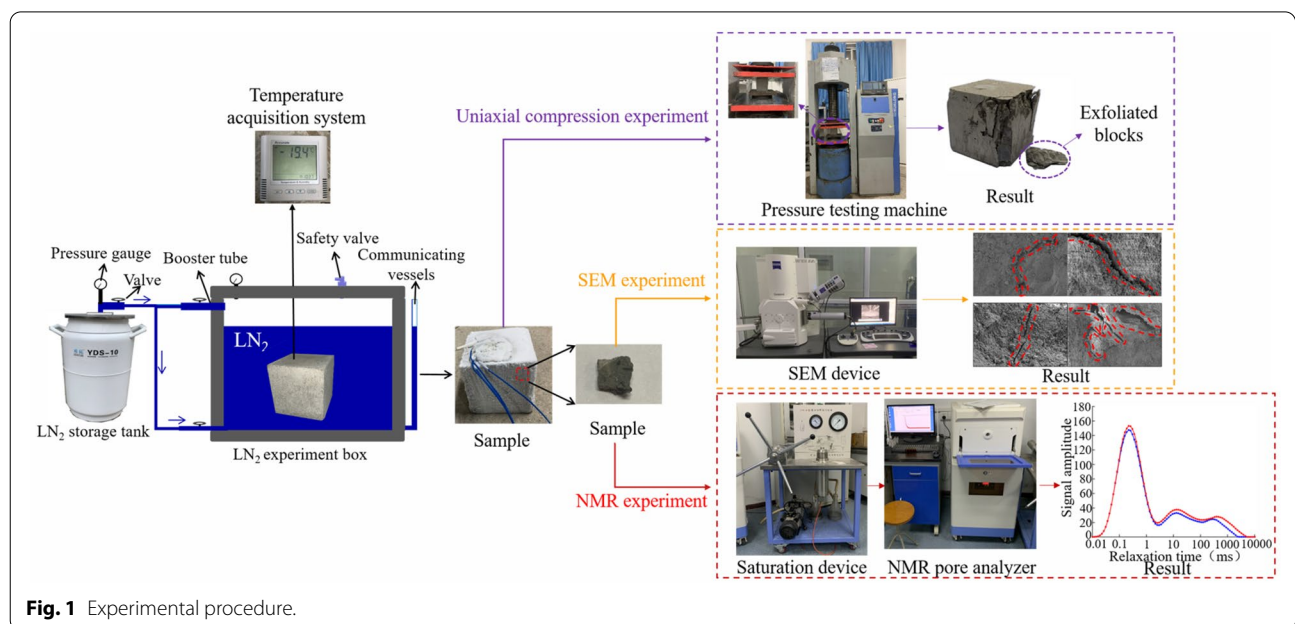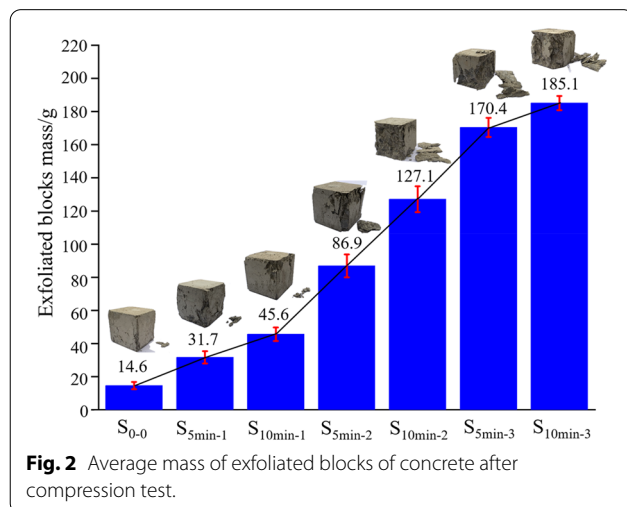

Fig. 1 Experimental procedure.

Liu *et al. Int J Concr Struct Mater*   (2021) 15:49

Page 4 of 12

cold shock for 5 min or 10 min, standing at environmental temperature to return to environmental temperature $(20\pm3\ °C)$, is a LN_2 freeze–thaw cycle. The number of cycles is expressed in numbers. For example, when LN_2 cold shock is for 5 min, the number of concrete samples treated in one cold shock cycle is S_{5min-1}, and the number of concrete samples treated in two cold shock cycles is S_{5min-2}.

2.2.2 Results Analysis
(1) Mass of exfoliated blocks of concrete.

Fig. 2 shows the average mass of the exfoliated blocks of concrete after the compressive test. It can be seen from Fig. 2 that the average mass of the exfoliated blocks of concrete after LN_2 cold shock continuously increased. Compared with the original sample, the average mass of exfoliated blocks for samples S_{5min-1}, S_{5min-2}, and S_{5min-3} increased by 2.2, 6.0, 11.7 times, respectively, and the average mass of exfoliated blocks for samples $S_{10min-1}$, and $S_{10min-2}$, $S_{10min-3}$ increased by 3.1, 8.7, 12.7 times, respectively. This is because many micro-cracks inside the concrete after the LN_2 cold shock are first generated. Then, they rapidly expanded and interpenetrated during the compressive test process so that a large number of exfoliated blocks are scaled off. Under the same shock cycles, the average mass of the exfoliated blocks of samples S_{5min-1} and $S_{10min-1}$ increased to some extent, which shows that the cold time has a certain positive effect on the mass of the exfoliated blocks. For both samples, S_{5min-2} and $S_{10min-1}$ with total cold shock time of 10 min, the average mass of the exfoliated blocks for $S_{10min-1}$ was significantly increased, and it can be concluded that more numbers of LN_2 cold shock cycles have the great increase on the average mass of the exfoliated blocks.
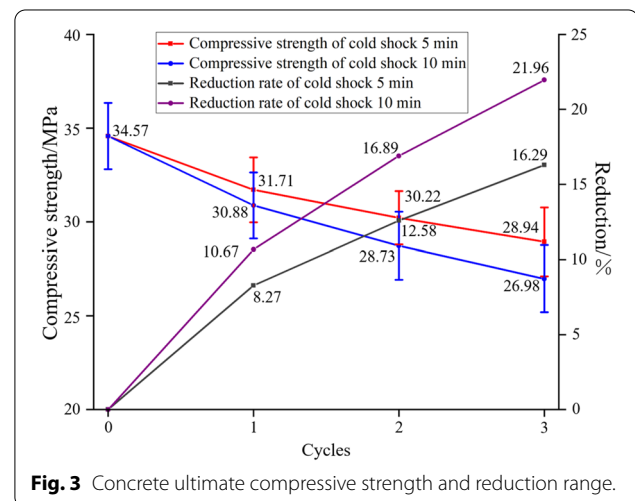
In the time range of this experiment, with the increase of cold shock time and the number of shock cycles, the internal micro-cracks of concrete formed, propagated and interpenetrated, inducing the larger total volume of the exfoliated blocks of concrete after uniaxial compression experiment. Eventually, with the effect of cumulative damage, the concrete integrity was reduced, causing the decrease of compressive strength.

(2) Changes in compressive strength.

① The effect of cold shock time.

The change curve in compressive strength of concrete before and after LN_2 cold shock is shown in Fig. 3. The compressive strength values of the samples for LN_2 cold shocks of 5 min and 10 min as well as 1, 2, and 3 shock cycles were decreased, compared with the original sample. The compressive strength values of samples S_{5min-1} and $S_{10min-1}$ decreased by 8.27% and 10.67%, respectively, compared with the original sample. Due to the relatively small porosity of the original sample, the original cracks were relatively small, and the crack space after LN_2 cold shock was greatly increased, resulting in severe damage to the concrete sample. Although the internal micro-cracks of concrete sample after LN_2 cold shock of 5 min initiate and expand, the frost heaving force and temperature stress cause relatively little expansion of the original cracks and the initiation of new cracks in the same period. Therefore, the compressive strength of the original sample with relatively small porosity had a great decrease on the compressive strength values of concrete sample after LN_2 cold shock. Finally, under the combined action of the cyclic frost heaving force and temperature stress, the compressive strength of sample $S_{10min-3}$ had a decrease of 5.77%, compared with sample S_{5min-3}.

② The effect of the number of shock cycles.

Fig. 2 Average mass of exfoliated blocks of concrete after compression test.

Fig. 3 Concrete ultimate compressive strength and reduction range.

Liu *et al. Int J Concr Struct Mater*   (2021) 15:49

Page 5 of 12

It can be seen from Fig. 3 that the compressive strength of the concrete with 3 LN_2 shock cycles decreased more significantly, and the compressive strength between $S_{10min-3}$ and $S_{10min-2}$ and that between $S_{10min-2}$ and $S_{10min-1}$ had the differences of 5.07% and 6.22%, respectively. The differences between S_{5min-3} and S_{5min-2} and between S_{5min-2} and S_{5min-1} were 3.61% and 4.31%, respectively. It can be found that as the number of shock cycles increased, the reduction rate of the compressive strength gradually decreased. This is because that as the number of shock cycles increased, the crack formation and expansion caused by frost heaving force and temperature stress were weakened, and the damage in concrete gradually decreased. Finally, with the cumulative damage, the reduction rate of the compressive strength was up to 21.96%.

2.3 Microscopic Failure Characteristics

To reveal the cracking mechanism of concrete after LN_2 cold shock, this section carried out the SEM scans and the NMR tests. It microscopically explained the physical nature of concrete deterioration after LN_2 cold shock by comparing the original samples.

2.3.1 Sample Preparation

The SEM test samples are cored by the core drilling machine after cold shock for 5 min or 10 min and cycling for 1, 2 and 3 times, then the core samples are cut into 3-mm-thick sheets, and subjected to SEM test after drying for 8 h. The NMR test samples are drilled using the water drilling method to shape cylindrical samples with a diameter of about 20 mm and a length of about 20 mm. The samples are taken out after cold shock for 5 min or 10 min and cycling for 1, 2 and 3 times, NMR test shall be carried out after water saturation for 12 h under water pressure of 20 MPa. The detailed parameters of NMR test are shown in Table 1 below.

2.3.2 Principle

The micro-failure characteristics of concrete are closely related to its internal microstructure and damage. The internal micromorphology of concrete is observed under SEM to obtain the morphological characteristics of micro-cracks, so as to analyze and judge the failure characteristics of concrete in the damage process (Nie et al., 2016; Qin et al., 2020). [1]H-saturated water in the pores of the tested object is used as the probe in NMR. The attenuation signals of H signal spin-echo strings in different pores in the matrix are integrated and inversed based on Carr–Purcell–Meiboom–Gill sequence (CPMG sequence), so as to determine the T_2 relaxation time spectrum of water signal in the matrix. The pore size and pore volume are positively correlated with the T_2 value and
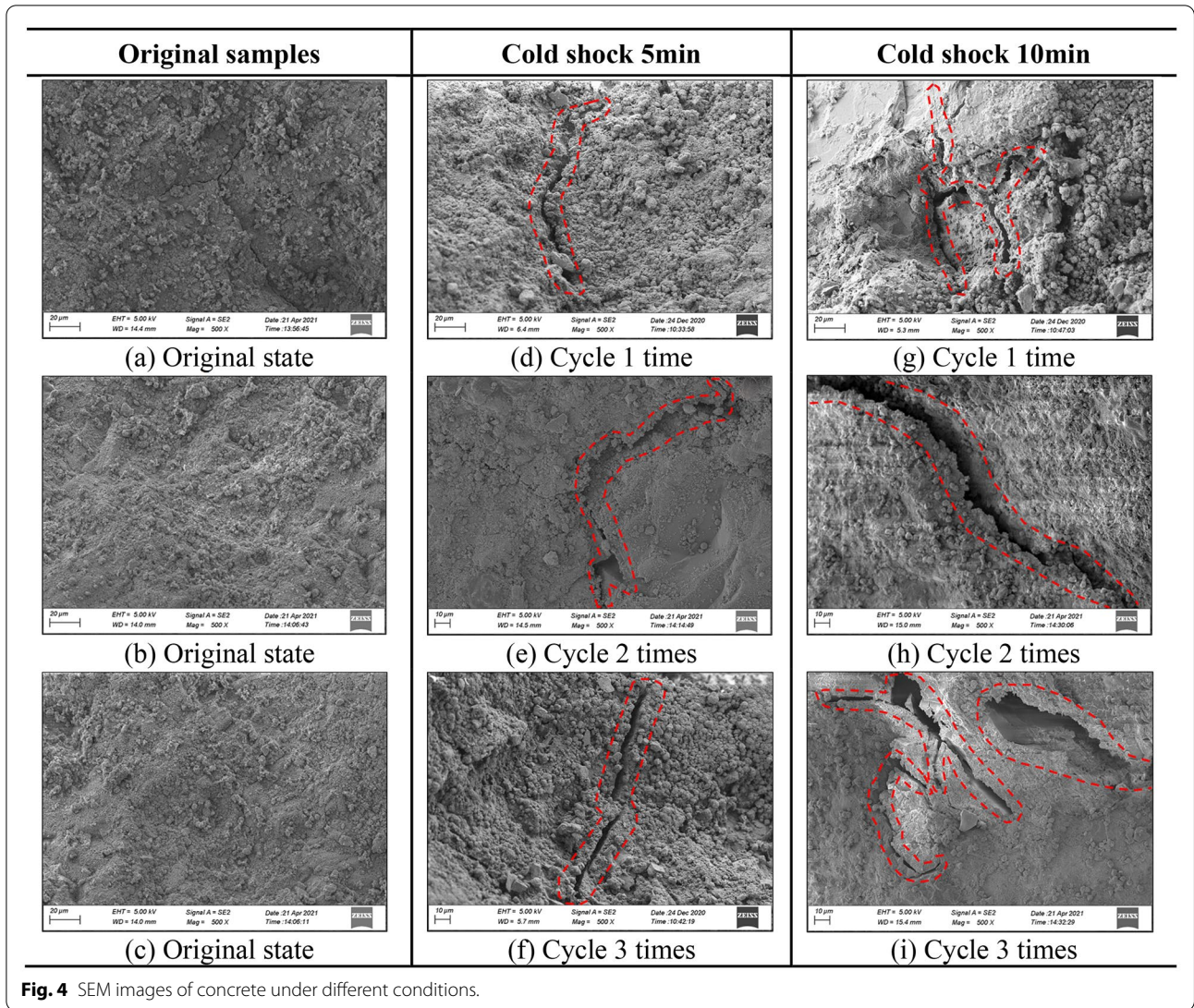
Table 1 NMR parameters applied in the test.

Parameters	Value
SEQ	CPMG
SF/MHz	20
O1/Hz	732,970.31
P1/us	5
TD	500,004
PRG	1
TW/ms	3000
P2/us	12
TE/ms	0.1
NECH	15,000
SW/KHz	333.333
RFD/ms	0.020
RG1(db)	20.0
DRG1	2
NS	16

the T_2 spectrum area, respectively, and mainly affected by the pore structure of concrete, the shape of the T_2 distribution curve of concrete with different pore structures of concrete have certain difference (Matteson et al., 2000). Therefore, the typical concrete samples before and after LN_2 cold shock were tested by SEM micro-scanning and NMR to study further the internal microstructure and internal pore changes of concrete samples.

2.3.3 Discussion

1. SEM

Fig. 4 displays typical SEM images with different LN_2 cold shock time. At the magnification of 500x, the internal structure of concrete before and after LN_2 cold shock had certain differences. Fig. 4a–c shows the test results of the original samples. It indicates that the original concrete sample had the relatively dense internal structure, only shallow cracks. Fig. 4d–f shows the test results of S_{5min-1}, S_{5min-2} and S_{5min-3}, respectively. It can be seen that when LN_2 cold shock lasts for 5 min, the crack gradually develops and the crack width increases. It indicates that the gain effect of LN_2 cold shock on crack development is obvious. Fig. 4g–I shows the test results of $S_{10min-1}$, $S_{10min-2}$ and $S_{10min-3}$, respectively. In the S_{10min} sample, a large number of micro-cracks penetrate each other to form a crack area, and the crack further expands to a larger width and depth. In addition to the above low temperature-induced fracturing, there are also local defects in the dense matrix, such as fracturing holes and loose exfoliated particles, which further increase the damage of the sample.
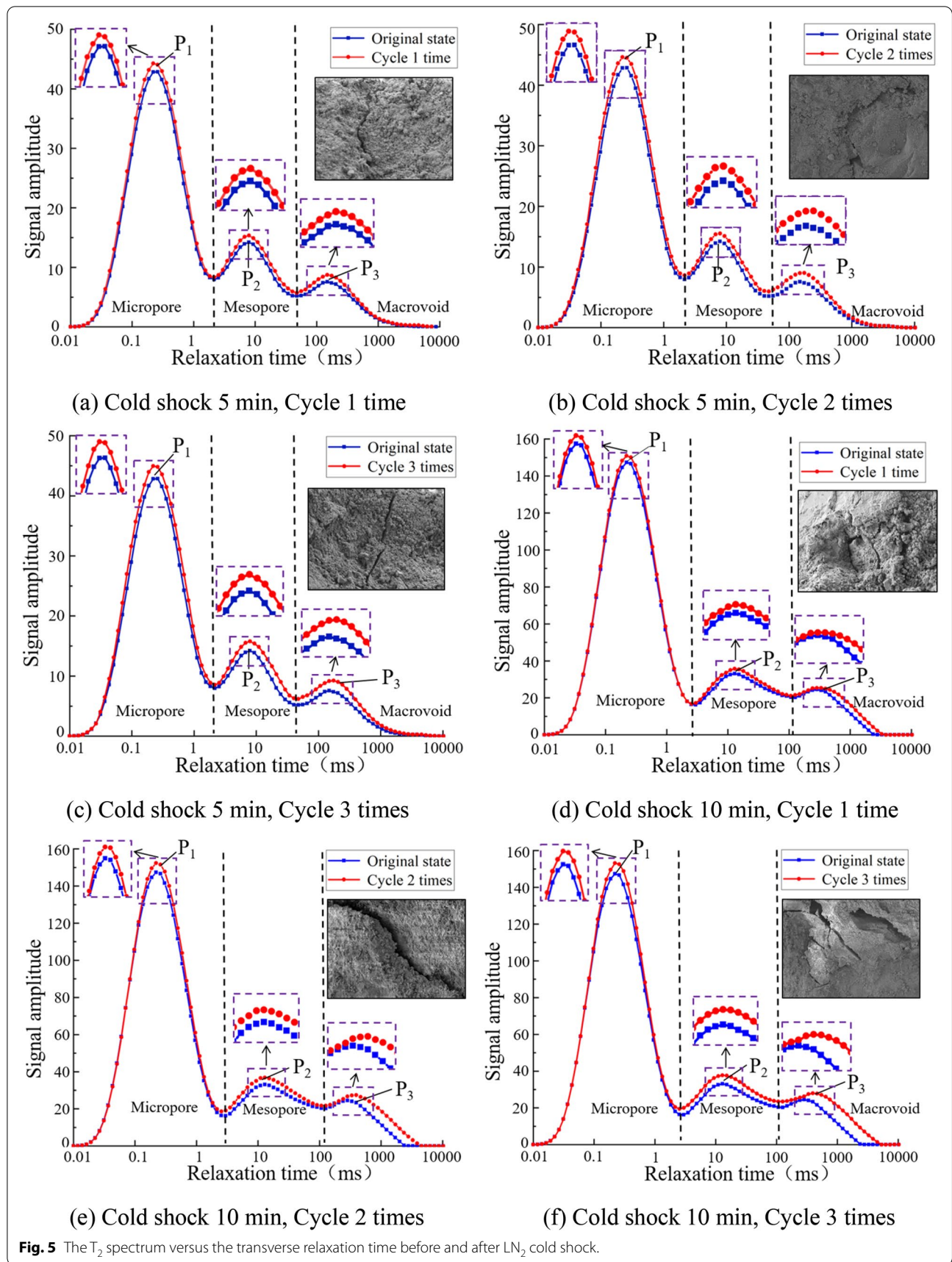
Original samples	**Cold shock 5min**	**Cold shock 10min**
(a) Original state	(d) Cycle 1 time	(g) Cycle 1 time
(b) Original state	(e) Cycle 2 times	(h) Cycle 2 times
(c) Original state	(f) Cycle 3 times	(i) Cycle 3 times

Fig. 4 SEM images of concrete under different conditions.

It can be concluded that micro-cracks were generated in two forms: one is that a large number of new cracks were derived, the other is that the original cracks propagated and interpenetrated to generate overall destruction of the concrete structure to a large extent.

2. NMR

① T_2 Distribution Changes Versus Transverse Relaxation Time

Fig. 5 shows the T_2 spectrum change versus the transverse relaxation time before and after LN_2 cold shock. It can be seen that under the combined action of frost heaving force and temperature stress, the spectral line of concrete sample after LN_2 cold shock moves along the positive direction of the time axis, and the

maximum relaxation time increases, compared with the original sample. The maximum transverse relaxation time of concrete samples S_0, S_{5min-1}, S_{5min-2} and S_{5min-3} is 5336 ms, 6280 ms, 7390 ms, and 8697 ms, respectively, and the maximum transverse relaxation time of concrete samples S_0, $S_{10min-1}$, $S_{10min-2}$ and $S_{10min-3}$ is 2364 ms to 3274 ms, 3853 ms, and 4534 ms, respectively, which reflect that the maximum transverse relaxation time increases with the increase of the number of shock cycles, and the combined action of frost heaving force and temperature stress induces new large-size pores inside concrete. Besides, it should be noted that the large difference in the signal amplitude of the T_2 spectrum in Fig. 5a–c and Fig. 5d–f is mainly caused by the difference in the pore structure of the sample. This research mainly compared T_2 spectrum versus the transverse relaxation time before and after the LN_2 cold

Fig. 5 The T_2 spectrum versus the transverse relaxation time before and after LN_2 cold shock.

Liu *et al. Int J Concr Struct Mater* (2021) 15:49

Page 8 of 12

shock of the same sample, the influence of the difference in scale on the test results can be ignored.

② Transverse Relaxation Time T_2 Spectral Area Change

Table 2 displays the T_2 spectrum area change of concrete sample in the saturated state. Compared with the original sample, the spectral area of the concrete sample after LN_2 cold shock increases in different rates, the increase rates of S_{5min-1}, S_{5min-2} and S_{5min-3} are 5.25%, 8.43%, and 10.36%, respectively, and the increase rates of $S_{10min-1}$, $S_{10min-2}$ and $S_{10min-3}$ are 7.51%, 11.97%, and 14.66%, respectively. The total area of the T_2 spectrum of the concrete sample after LN_2 cold shock shows an overall upward trend. Additionally, the changes of different peak areas before and after LN_2 cold shock can determine the specific damage process and form of concrete caused by the combined effect of frost heaving force and temperature stress.

It can be seen from Table 2 that the proportion of the first peak area decreases, which indicates that the proportion of micro-pores in the concrete decreases. And the proportions of the areas of second peak and third peak increase, indicating that the micro-pores expand and connect each other to induce large-sized pores. It can be concluded that concrete damage after LN_2 cold shock is mainly reflected on the development and expansion of micro-pores, the micro-pores propagate and connect with each other to form large-sized pores, and finally cause the reduction of concrete integrity.

3. Destruction mechanism

Fig. 6 shows the deterioration mechanism of concrete strength under LN_2 cold shock. When concrete was immersed in LN_2, due to the poor thermal conductivity of concrete, a certain temperature gradient was formed inside the concrete, and the temperature of the

concrete would instantly decrease. According to the Jennite molecular model, it can be found that there were certain amount of water molecules in concrete, and the water molecules transformed from the disordered state phase to the regular state of ice molecules, therefore the volume of water would expand by about 9% when the water was turned into ice, and an expansion pressure of 207 MPa was formed theoretically (Qin, 2018). The volume expansion of water in the pores would compress the pore wall and caused the frost heaving damage of concrete. Additionally, the LN_2 cold shock involved a process from rapid cold shock and shrinking to heating up and expansion, leading to the generation of sufficient thermal stress between cement mortar and aggregates, causing further expansion of original cracks. When the thermal stress value exceeded the bonding strength of micro-unit between the materials, the microstructure of the concrete was destroyed and new micro-cracks were formed. Because there is a significant difference in intensity between cement mortar and aggregate, it is easy for cement mortar to firstly occur failure under the combined action of temperature stress and frost heaving force.
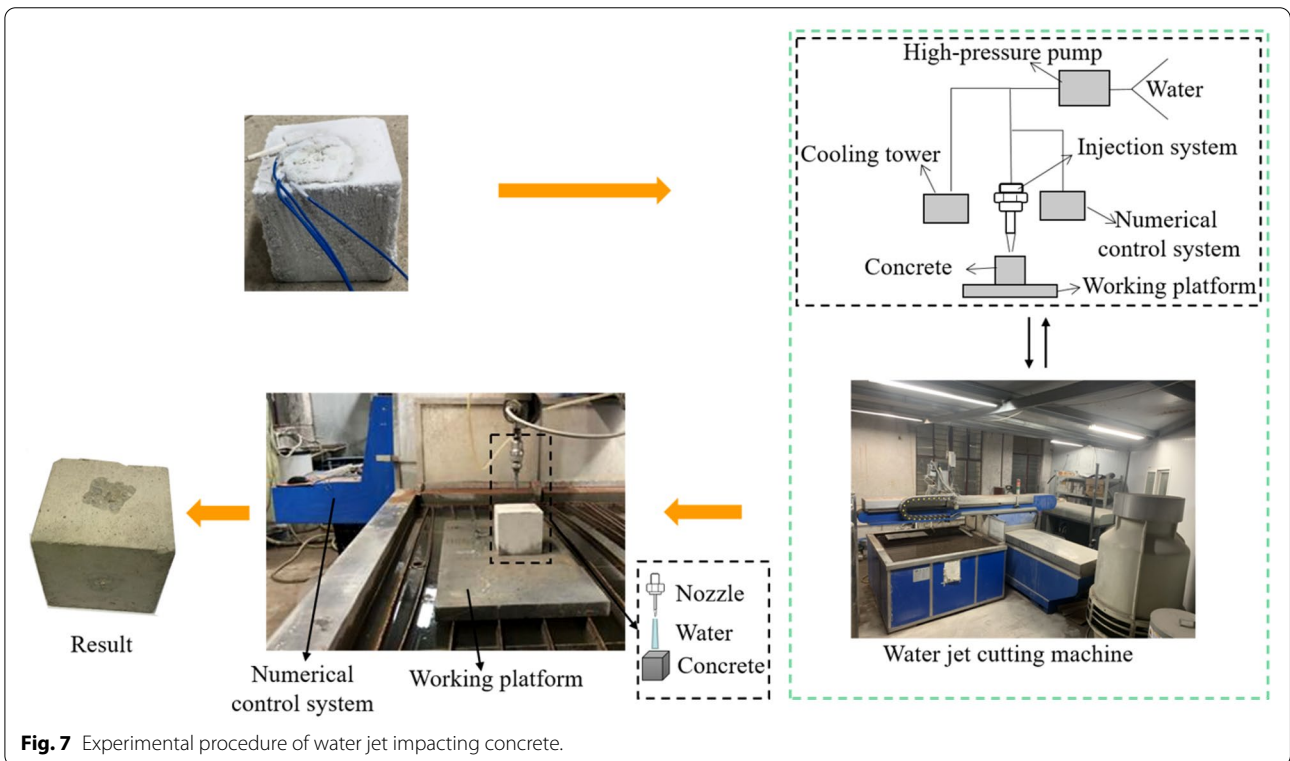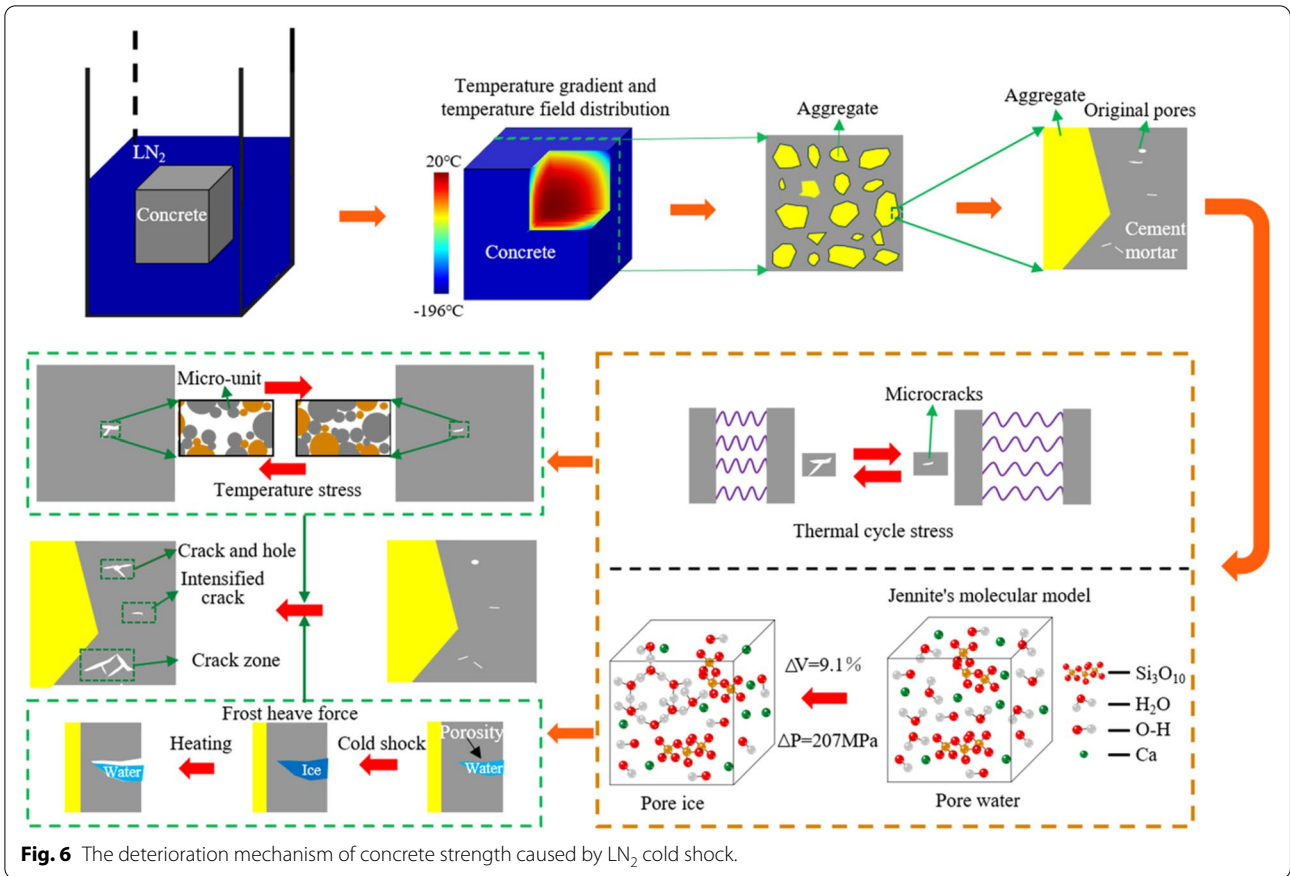
3 Water Jet Impact Experiment

Through the compression test of concrete after LN_2 cold shock, the failure characteristics of and microscopic failure mechanism of concrete were revealed. To further reveal the failure characteristics of the water jet crushing concrete after LN_2 cold shock, the water jet impact experiment was carried out.

3.1 Devices and Sample Preparation

To study the effect of LN_2 on the high-pressure water jet crushing concrete, the water jet machine applied in the impact experiment was the impact system of Shanghai JINJIAN JJ-I42*1313. In the experiment, the same batch

Table 2 The T_2 spectrum area change of the concrete sample after LN_2 cold shock.

Number of cycles	Total area of spectrum		Change rate/%	First peak ratio/%		Second peak ratio/%		Third peak ratio/%	
	Original state	After the test		Original state	After the test	Original state	After the test	Original state	After the test
Cold shock 5 min									
1	966.96	1017.72	5.25	67.009	65.905	20.896	21.613	12.095	12.482
2	966.96	1048.43	8.43	67.009	65.118	20.896	21.847	12.095	13.035
3	966.96	1067.16	10.36	67.009	64.272	20.896	22.142	12.095	13.586
Cold shock 10 min									
1	3248.27	3492.12	7.51	70.312	68.271	16.995	17.874	12.693	13.855
2	3248.27	3637.09	11.97	70.312	67.537	16.995	18.225	12.693	14.238
3	3248.27	3724.51	14.66	70.312	66.429	16.995	18.752	12.693	14.819

Fig. 6 The deterioration mechanism of concrete strength caused by LN_2 cold shock.

Fig. 7 Experimental procedure of water jet impacting concrete.

Liu *et al. Int J Concr Struct Mater*   (2021) 15:49

Page 10 of 12

of C30 concrete samples after LN_2 cold shock of 5 min and 10 min are selected as the research objects. The experimental procedure is demonstrated in Fig. 7.

3.2 Analysis of Experimental Results

It can be found from Fig. 8 that under the impact conditions of the jet pressure of 150 MPa and the impact time of 10 s, the crater had the irregular shape and the unsmooth opening, with the uneven wall surface and obvious erosion marks of water jet. The maximum widths of craters for samples S_0, S_{5min} and S_{10min} were 12.37 mm, 17.54 mm and 21.86 mm, respectively, and the maximum perforation depths of them were 3.76 mm, 4.53 mm and 5.28 mm, respectively. And the maximum width and maximum depth of the crater of concrete after LN_2 cold shock greatly increased. Compared with the original sample, the maximum width and depth of the crater for sample S_{5min} increased by 41.79% and 20.48%, respectively, and the maximum width and depth of the crater for sample S_{10min} increased by 76.72% and 40.43%, respectively, which indicate that concrete sample after the LN_2 cold shock has wider expansion of the crater along surroundings when it is impacted by the water jet. Besides, with the increase of cold shock time, the water jet's breaking range and failure volume became larger. This is because that a large number of cracks in the concrete sample after LN_2 cold shock develop to decrease the bond force, and the water jet immerses in the cracks to form a water wedge effect under dynamic pressure of water jet. The coupling effect of the weakened bond force and the water wedge effect causes the greater damage degree of concrete sample after LN_2 cold shock, compared with the original sample. According to Fig. 9, under the impact conditions of the jet pressure of 200 MPa and the impact time of 10 s, the maximum widths of craters for samples S_0, S_{5min} and S_{10min} were 15.36 mm, 20.19 mm, 25.13 mm, and the maximum perforation depths of them were 3.97 mm, 5.82 mm, and 6.14 mm, respectively. By comparison, it is found that the crushing range and depth of craters for sample S_{5min} under jet pressure of 150 MPa were greater than that of sample S_0 under jet pressure of 200 MPa. Results show that the LN_2 cold shock can effectively increase the water jet's breaking range and failure volume and improve the energy utilization rate.

The experimental results show that under the same pump pressure, the LN_2 assisted water jet crushing can cause a larger broken area and a wider range of damage. In the emergency demolition process, especially some concrete structures that are difficult to dismantle, it can realize rapid and large-volume crushing by coupling LN_2 cold shock and high-pressure water jet impact. Besides, in the demolition process, LN_2 can cause severe damage to large concrete structures, produce complex microcracks in the concrete structures, and expand the volume of the reconstruction.

4 Conclusion

Based on the mechanical test, scanning electron microscopy (SEM), and nuclear magnetic resonance (NMR) technology, this paper revealed changes in the
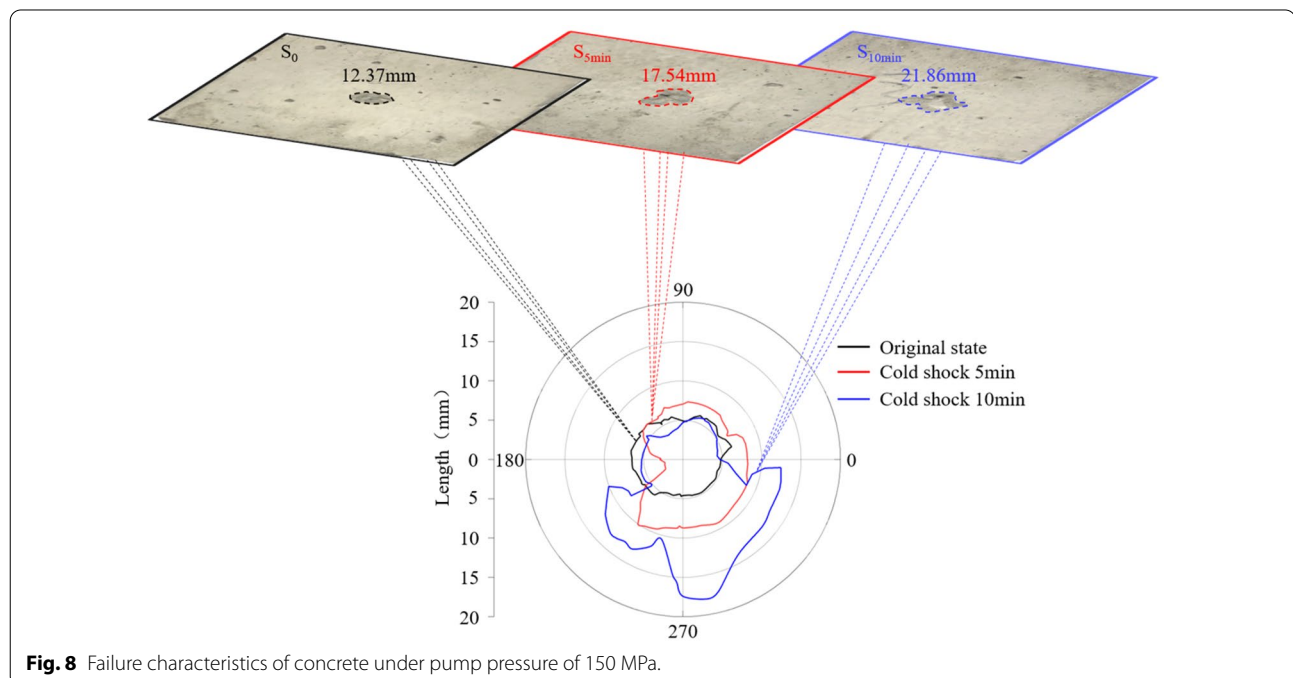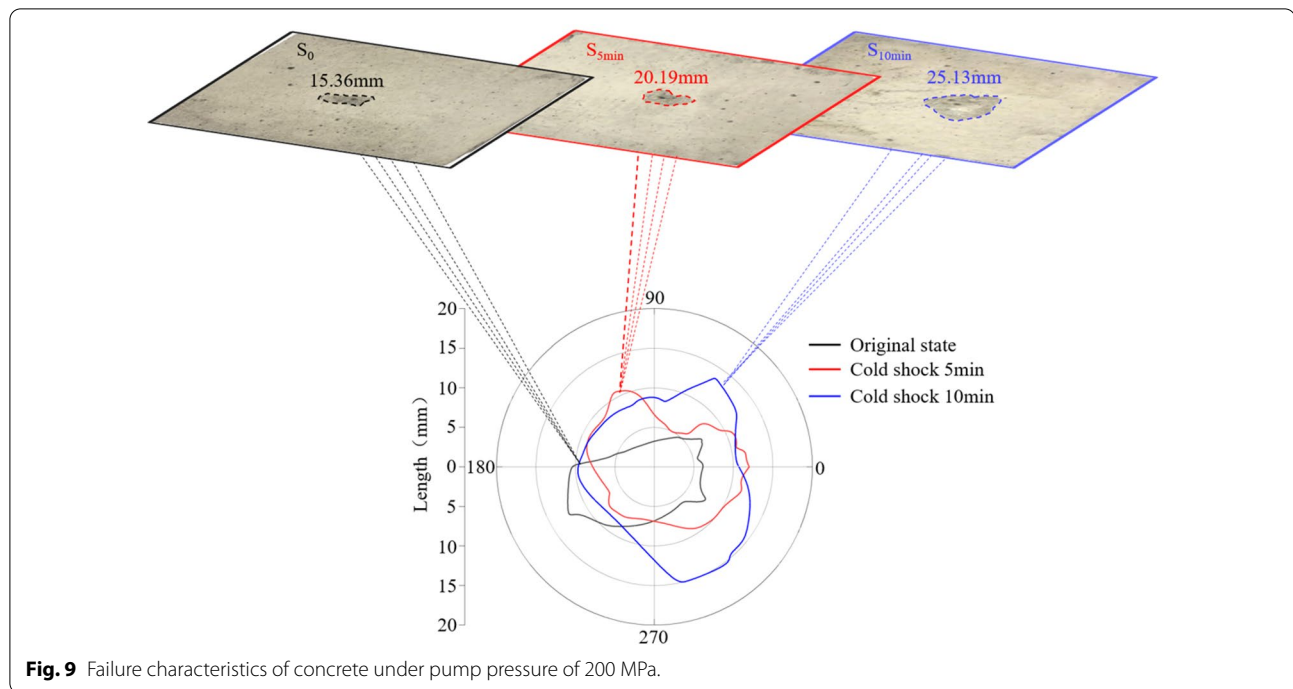

Fig. 8 Failure characteristics of concrete under pump pressure of 150 MPa.

Liu *et al. Int J Concr Struct Mater*   (2021) 15:49

Page 11 of 12

Fig. 9 Failure characteristics of concrete under pump pressure of 200 MPa.

mechanical properties, characteristics of internal microscopic failure and internal pore changes of the concrete before and after LN_2 cold shock. The main conclusions are shown as follows:

1. With the increase of cold shock time and shock cycles, the total volume of the exfoliated blocks after compression failure expanded, and the average mass of the exfoliated blocks is 2.2 times to 12.7 times bigger compared with that of the original sample. The number of shock cycles has a greater effect on the average mass of the exfoliated blocks than the cold shock time. LN_2 cold shock can effectively reduce the uniaxial compressive strength of concrete, and the uniaxial compressive strength decreases by 8.27%–21.96%.

2. Based on SEM scans, it is found that LN_2 cold shock can cause more micro-cracks to develop inside the concrete, and the expansion degree of micro-cracks increases as the cold shock time increases.

3. Through NMR test, it is indicated that LN_2 cold shock can increase the internal porosity of concrete and generate larger pores, the longer the cold shock effect, the higher the development degrees of pores are.

4. Under the condition of jet pressure of 150 MPa, the maximum width and depth of the crater for concrete sample S_{5min} increase by 41.79% and 20.48%, and the maximum width and depth of crater for sample S_{10min} increase by 76.72% and 40.43%, compared with the original sample. The crushing range and depth of sample S_{5min} under jet pressure of 150 MPa are greater than S_0 under jet pressure of 200 MPa. It indicates that LN_2 assisted water jet crushing concrete can effectively increase the breaking range and failure volume of water jet, improve the energy utilization rate, and expand the reconstruction volume.

Authors' contributions
JL contributed to the conception of the study; YJ performed the experiment; YZ contributed significantly to analysis and manuscript preparation; JL performed the data analyses and wrote the manuscript; XZ helped perform the analysis with constructive discussions; CT gave guidance in the experiment. All authors read and approved the final manuscript.

Authors' information
Jialiang Liu: Associate professor, State Key Laboratory of Mountain Bridge and Tunnel Engineering, Chongqing Jiaotong University, Chongqing 400074, People's Republic of China; Associate professor, Civil Engineering College, Chongqing Jiaotong University, Chongqing 400074, People's Republic of China; Post-doctoral, Chongqing Energy Investment Group Science & Technology Co., LTD, Chongqing 400061, People's Republic of China. Yu Jin: Master's Student, Civil Engineering College, Chongqing Jiaotong University, Chongqing 400074, People's Republic of China. Yujie Zhu: Master's Student, Civil Engineering College, Chongqing Jiaotong University, Chongqing 400074,

Liu *et al. Int J Concr Struct Mater*   (2021) 15:49

Page 12 of 12

People's Republic of China. Jinyang Li: Master's Student, Civil Engineering College, Chongqing Jiaotong University, Chongqing 400074, People's Republic of China. Xuguang Zhang: Doctor, Chongqing Jianzhu College, Chongqing 400072, People's Republic of China. Chao Tao: Engineer, Chongqing Jiaotong University Traffic Safety Science and Technology Research Institute Company Limited, Chongqing 400074, People's Republic of China.

Funding

Availability of data and materials
The datasets used or analyzed during the current study are available from the corresponding author on reasonable request.

Declarations

Competing interests
The authors declare no conflicts of interest.

Author details
[1]State Key Laboratory of Mountain Bridge and Tunnel Engineering, Chongqing Jiaotong University, Chongqing 400074, People's Republic of China. [2]Civil Engineering College, Chongqing Jiaotong University, Chongqing 400074, People's Republic of China. [3]Chongqing Energy Investment Group Science & Technology Co., LTD, Chongqing 400061, People's Republic of China. [4]Chongqing Jianzhu College, Chongqing 400072, People's Republic of China. [5]Chongqing Jiaotong University Traffic Safety Science and Technology Research Institute Company Limited, Chongqing 400074, People's Republic of China.

References
Abdulagatova, Z. Z., Kallaev, S. N., Omarov, Z. M., Bakmaev, A. G., Grigor, E. B. A., & Abdulagatov, I. M. (2019). Temperature effect on thermal-diffusivity and heat-capacity and derived values of thermal-conductivity of reservoir rock materials. *Geomechanics and Geophysics for Geo-Energy and Geo-Resources, 6*(B5), 3586–3593.

Cai, C. Z., Li, G. S., Huang, Z. W., Shen, Z. H., Tian, S. C., & Wei, J. W. (2014). Experimental study of the effect of liquid nitrogen cooling on rock pore structure. *Journal of Natural Gas Science and Engineering, 21*, 507–517.

Cha, M., Yin, X., Kneafsey, T., Alqahtani, N., Miskimins, J., Patterson, T., Wu, Y., & S. (2014). Cryogenic fracturing for reservoir stimulation-Laboratory studies. *Journal of Petroleum Science and Engineering, 124*, 436–450.

Cheng, Y. F., Jiang, L., Wang, H. D., & Ubedullah, A. (2017). Experimental study on pore structure and mechanical properties of stratified coal. *International Journal of Geomechanics, 17*(12), 04017116.

Hartell, J. A., & Zeng, H. (2020). Concrete degradation due to moisture and low- and high-temperature cycling. *ACI Materials Journal, 117*(1), 129–138.

Hou, C. P., Chen, D., & H., Peng, G., Liu, C. Y., & Wu, C. (2020). Study on dynamic axial compression constitutive characteristics of freezing-thawing deteriorated concrete in frozen state. *Journal of Experimental Mechanics, 35*(06), 1101–1112.

Huang, Z. W., Wei, J. W., Li, G. S., & Cai, C. Z. (2016). An experimental study of tensile and compressive strength of rocks under cryogenic nitrogen freezing. *Rock and Soil Mechanics, 37*(03), 694–700.

Jiang, Z., He, B., Zhu, X., Ren, Q., & Zhang, Y. (2020). State-of-the-art review on properties evolution and deterioration mechanism of concrete at cryogenic temperature. *Construction and Building Materials, 257*, 119456.

Justo, J., Castro, J., & Cicero, S. (2020). Notch effect and fracture load predictions of rock beams at different temperatures using the theory of critical distances. *International Journal of Rock Mechanics and Mining Sciences, 125*, 104161.

Marshall, A. L. (1982). Cryogenic concrete. *Cryogenics, 22*(11), 555–565.

Matteson, A., Tomanic, J. P., Herron, M. M., Allen, D. F., & Kenyon, W. E. (2000). NMR relaxation of clay/brine mixtures. *SPE Reservoir Evaluation & Engineering, 3*(5), 408–413.

Nie, L., Xu, J. Y., Liu, Y. F., Fan, J., & s., & Wang, H. W. (2016). Strength change regularity and micro-structure analysis of concrete in sulfate environment. *Journal of Vibration and Shock, 35*(20), 203–208.

Penttala, V., & Fahim, A. (2002). Stress and strain state of concrete during freezing and thawing cycles. *Cement and Concrete Research, 32*(9), 1407–1420.

Pu, Q., Xue, W. Y., Jiang, L. H., Xi, F. D., Zhang, C. Z., Dai, D. L., & Xie, X. R. (2020). Research on the fracture damage characteristics of concrete under freeze thaw cycle. *China Concrete and Cement Products, 07*, 30–33.

Qin, L. (2018). Pore evolution after fracturing with cyclic liquid nitrogen and the mechanism of permeability enhancing. *China University of Mining & Technology.*

Qin, L., Zhai, C., Liu, S. M., Xu, J. Z., Yu, G. Q., & Sun, Y. (2017). Changes in the petrophysical properties of coal subjected to liquid nitrogen freeze-thaw—A nuclear magnetic resonance investigation. *Fuel, 194*, 102–114.

Qin, Y., Xu, B., & Zheng, Y. F. (2020). Experimental study on freezing and thawing failure test of diatomite doped concrete with pore structure. *Subgrade Engineering, 05*, 43–48.

Thomas., J., M., & Alan, L. (2019). Compressive stress-strain response of concrete exposed to low temperatures. *Journal of Cold Regions Engineering, 33*(4), 04019014.

Yang, Y., Li, X. L., Yang, R. S., & Wang, J. G. (2020). Study on fractal characteristics and fracture mechanism of frozen rocks. *Transaction of Beijing Institute of Technology, 40*(06), 632–639.

Yuan, J. W., & Chang, D. (2020). Contrast test of liquid nitrogen freeze-thaw cycle cracking effect between anthracite and coking coal. *Coal Science and Technology, 48*(12), 141–147.

Zhai, C., Qin, L., Liu, S., & Xu, J. Z. (2016). Pore structure in coal: Pore evolution after cryogenic freezing with cyclic liquid nitrogen injection and its implication on coalbed methane extraction. *Energy & Fuels, 30*, 6009–6020.

Zhai, C., & Xu, J. Z. (2020). Research on cyclic liquid nitrogen fracturing technology for enhancing coalbed methane drainage and its application prospect. *Industry and Mine Automation, 46*(10), 1–8.

Zhang, L., Tian, M. M., Xue, J. H., Li, M. X., Zhang, C., & Lu, S. (2021). Effect of liquid nitrogen cycle treatment on seepage characteristics of coal samples with different water contents. *Journal of China Coal Society, 1*, 1–11.

Zhu, X., Jiang, Z., He, B., & Qian, C. (2020). Investigation on the physical stability of calcium-silicate-hydrate with varying CaO/SiO_2 ratios under cryogenic attack. *Construction and Building Materials, 252*, 119103.

Zhu, X., Qian, C., He, B., Chen, Q., & Jiang, Z. (2020). Experimental study on the stability of C-S-H nanostructures with varying bulk CaO/SiO_2 ratios under cryogenic attack-ScienceDirect. *Cement and Concrete Research, 135*, 106114.

Publisher's Note